Journal of Solid State Chemistry **142,** 440–450 (1999)
Article ID jssc.1998.8064, available online at http://www.idealibrary.com on IDEAL®

Anion Ordering in Fluorinated La_2CuO_4

A. M. Abakumov,*,† J. Hadermann,* G. Van Tendeloo,* R. V. Shpanchenko,†
P. N. Oleinikov,† and E. V. Antipov†

**EMAT, University of Antwerp (RUCA), Groenenborgerlaan 171, B-2020 Antwerp, Belgium; †Department of Chemistry, Moscow State University, 119899 Moscow, Russia*

Received May 27, 1998; in revised form October 11, 1998; accepted October 12, 1998

La_2CuO_4 has been fluorinated using XeF_2 as a soft fluorinating agent at temperatures ranging from 200 to 400°C. The structure of the fluorinated samples was studied by a combination of X-ray diffraction (XRD), electron diffraction (ED), high-resolution electron microscopy (HREM), and microanalysis. XRD shows the sequential changes with increasing temperature of the XeF_2 treatment. A significant structural rearrangement, associated with the formation of a tetragonal K_2NiF_4-type structure (I-centered lattice with cell parameters $a = 4.0383(6)$ Å, $c = 13.093(3)$ Å) occurs at 250°C. Samples annealed at 300 and 400°C reveal the formation of a new monoclinic phase ($a \approx 17.36$ Å, $b \approx 5.62$ Å, $c \approx 10.59$ Å, $\beta \approx 91.5°$; SG, *C*2/*m*). The structural model, deduced from ED and HREM, involves the filling of part of the interstitial positions by fluorine atoms with removal of the neighboring oxygen, resulting in the formation of a fluorite-like arrangement of the La(O, F) layers. The fluorite-type and NaCl-type slabs alternate along the [110] direction of the K_2NiF_4 subcell in an ordered array. Several crystallites also show an incommensurate superstructure which is explained as a pseudoperiodic arrangement of shear planes. © 1999 Academic Press

INTRODUCTION

Stoichiometric La_2CuO_4 exhibits a semiconducting behavior. The hole concentration, which is necessary for the appearance of superconductivity, may be achieved either by heterovalent cationic substitution on the A-sublattice (1) or by the insertion of additional anions into the interstitial positions between the double LaO layers using a large variety of different techniques: high oxygen pressure annealing (2, 3), electrochemical oxidation, oxidation by a $KMnO_4$ solution (4, 5), and fluorination (6–8). La_2CuO_4 treated by diluted or pure F_2 gas reveals a superconducting transition with $T_c \approx 35$–40 K (6). The formation of a superconducting oxyfluoride was observed only for a low fluorination level, which is associated with a low temperature of the fluorine treatment (150–200°C). Earlier investigations were mainly devoted to the structural aspects of fluorine accommodation for this superconducting oxyfluoride. It was found that incorporation of a small amount of fluorine into the La_2CuO_4 structure (up to a $La_2Cu(O,F)_{4.18}$ composition) is accompanied by an enhancement of the orthorhombic distortion and an increase of the *c* parameter of the unit cell (7). Neutron powder structure refinement as well as EXAFS studies revealed that no significant structural transformation occurs during the fluorination; fluorine atoms are located at interstitial positions, tetrahedrally coordinated by La atoms and placed between two successive LaO layers (8). This behavior is similar to that previously found for oxygen-doped La_2CuO_4 samples (9).

An increase of the fluorination temperature leads to a structural rearrangement. The formation of a new non-superconducting tetragonal phase with cell parameters $a = 5.7(1)$ Å and $c = 13.1(1)$ Å was observed by X-ray diffraction when La_2CuO_4 was treated by F_2 at 230°C (10). Electron diffraction revealed the presence of a superstructure indexed on the basis of a monoclinic unit cell (11). An incommensurate superstructure connected with the formation of shear planes was also found in limited regions of the sample. The origin of this ordering was not determined, however, and the structure of the compound formed at a high level of fluorination is still unclear.

Recently we showed that XeF_2 is a soft and effective fluorinating agent and may be applied for the preparation of different superconducting oxyfluorides (12–15). In this paper we report the results of the fluorination of La_2CuO_4 by XeF_2 at different synthesis conditions and the structural characterization of the materials by a combination of X-ray diffraction, electron diffraction, and high resolution electron microscopy.

EXPERIMENTAL

La_2CuO_4 for further fluorination was prepared by a routine ceramic technique using La_2O_3 and CuO as initial reagents. Stoichiometric amounts of these oxides were intimately mixed, pressed into pellets, and heated in air at

0022-4596/99 $30.00

950°C for 40 h. The obtained monophasic La_2CuO_4 exhibits unit cell constants $a = 5.3562(2)$ Å, $b = 5.4015(2)$ Å, $c = 13.1531(8)$ Å, which are in good agreement with those previously published.

Since XeF_2 is very sensitive to the traces of moisture, all operations were carried out in a glove box filled with dried N_2. La_2CuO_4 (0.4 g) was mixed with XeF_2 (provided by the Laboratory of Inorganic Synthesis of the Institute of Applied Chemical Physics "Kurchatovskii Institut," Moscow, Russia) in a molar ratio of 1:1 and ground in an agate mortar. The mixture was placed in a Ni crucible and then sealed in a copper tube. The samples were annealed at temperatures ranging from 200 to 400°C for 40 h and then furnace cooled to room temperature.

The phase composition of the samples and the lattice parameters of the compounds were determined by X-ray diffraction using a focusing Guinier-camera FR-552 ($CuK\alpha_1$-radiation, germanium internal standard) and a Philips X'pert diffractometer ($CuK\alpha$-radiation, reflection geometry, proportional counter).

AC susceptibility measurements were performed in the temperature range 12–100 K at an external field amplitude of 1 Oe and a frequency of 27 Hz.

Electron diffraction (ED) and high resolution electron microscopy (HREM) were performed using a JEOL 4000EX instrument. EDX analysis and electron diffraction were performed using a Philips CM20 microscope with a LINK-2000 attachment. Image simulation was made using MacTempas software.

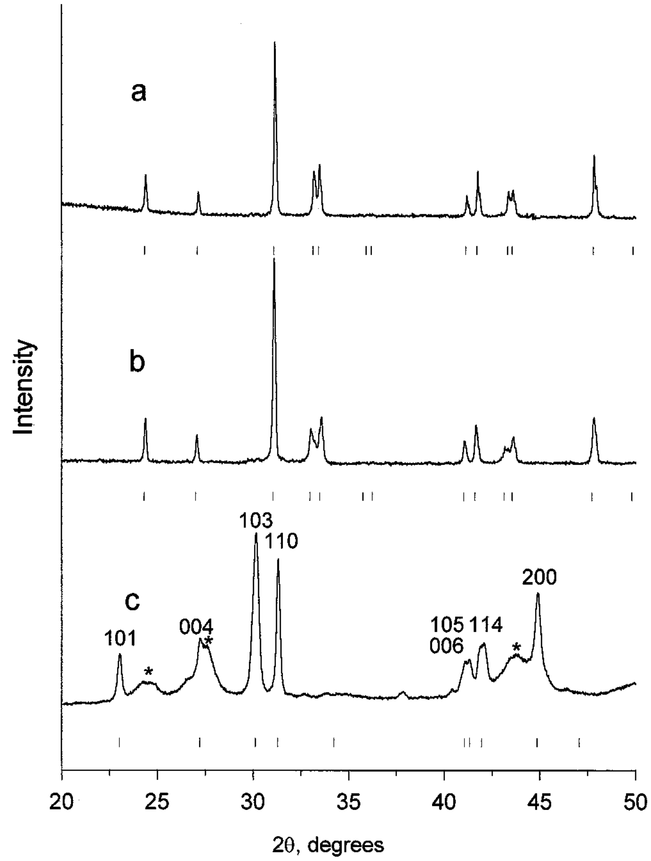

FIG. 1. X-ray diffraction patterns for (a) the initial La_2CuO_4 (b) fluorinated at 200°C and (c) fluorinated at 250°C. The theoretical peak positions were calculated using the cell dimensions described in the text; they are marked below. The peaks from LaOF are indicated by an asterisk.

RESULTS

X-ray diffraction patterns of fluorinated samples show clear changes with increasing temperature of the XeF_2 treatment (Fig. 1). A phase with a La_2CuO_4-type structure was obtained when the fluorination was performed at 200°C (Fig. 1b). The X-ray pattern was indexed as orthorhombic with cell parameters $a = 5.3526(4)$ Å, $b = 5.4239(5)$ Å, and $c = 13.206(1)$ Å. This compound exhibits an increased orthorhombic distortion in comparison with the initial La_2CuO_4, as is clear from the increased splitting of the 020 and 200 reflections with respect to the initial La_2CuO_4 (Fig. 1a). In fact, the cell parameters for the fluorinated compound obtained in our case are close to those observed before by different authors for superconducting fluorinated La_2CuO_4 (7, 8). Since the structure of this compound has been thoroughly studied already, no further investigation was performed.

A significant structural transformation with the formation of a tetragonal K_2NiF_4-type structure ($a = 4.0383(6)$ Å, $c = 13.093(3)$ Å; SG, $I4/mmm$) occurs after 250°C fluorination (Fig. 1c). Extremely wide peaks, visible on the X-ray pattern, correspond to badly crystallized LaOF oxyfluoride. Besides the reflections belonging to the tetragonal phase and LaOF, several broad reflections with weak intensities were also detected. The reflections of the main tetragonal phase within a limited 2θ-range exhibit significantly different broadening (for instance, 103 and 110 reflections). This different broadening as well as the presence of unindexed weak reflections points toward a decrease in symmetry and a deviation from the undistorted tetragonal unit cell. The X-ray diffraction pattern and cell dimensions for this compound are very similar to those previously observed for La_2CuO_4 fluorinated at 230°C by F_2 (10) if the increase of the a parameter by $\sqrt{2}$ would be taken into account (4.038 Å $\times \sqrt{2} = 5.71$ Å). However, we did not find any additional reflections which could lead to an increase of the a parameter.

Measurements of the temperature dependence of the magnetic susceptibility revealed that all samples fluorinated at temperatures above 200°C do not exhibit a superconducting transition down to 12 K, while samples treated at $t = 200$°C showed superconductivity with $T_{c,\,onset} \approx 40$ K.

The fluorine content of the crystallites was investigated inside the electron microscope using EDX analysis. An

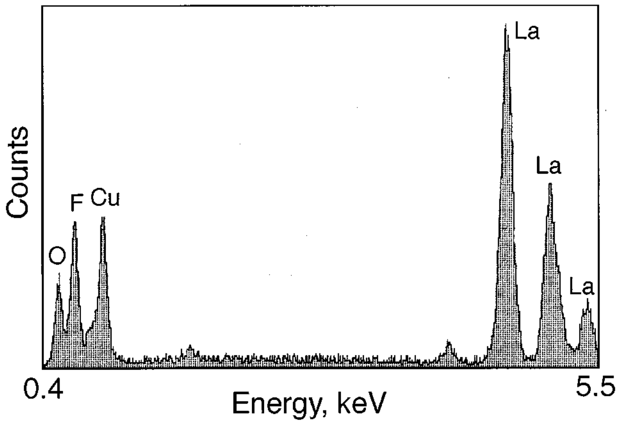

FIG. 2. Part of the EDX spectrum for the 250°C fluorinated sample showing $O(K_\alpha)$ and $F(K_\alpha)$ peaks in the lower energy range.

exact quantitative analysis of the fluorine content is difficult because of the low Z-number. A typical EDX spectrum in Fig. 2 clearly shows the presence of fluorine *within* the crystallites, but give only a rough estimation of the amount of fluorine incorporated.

To reveal the structural changes related to the fluorination, samples obtained at 250, 300, and 400°C were studied by ED and HREM. All electron diffraction reflections could be divided into two categories: the brighter spots were successfully indexed on the base of a body-centered tetragonal unit cell with cell dimensions close to those of the tetragonal K_2NiF_4-type phase by X-ray diffraction. Apart from these spots, belonging to the K_2NiF_4-sublattice, less bright superstructure reflections were found (see Fig. 3).

After a 250°C treatment, electron diffraction patterns along the $[100]_t^*$ and $[\bar{1}10]_t^*$ directions show weak superstructure reflections which were indexed on a body-centered tetragonal lattice with doubled cell parameters of the K_2NiF_4-subcell ($a = 8.06$ Å, $c = 26.2$ Å) (Fig. 3). The weakness of the superstructure spots and their unstability under electron beam irradiation allows us to connect them to an ordering on the anion sublattice. These circumstances hamper the direct observation of the ordering by HREM. The optical diffraction pattern, obtained from a $[\bar{1}10]_t$ HREM image shown in Fig. 4, reveals that the repeat period is 5.7 Å along $[110]_t$ and 13.1 Å along the $[001]_t$ axis. Since the unit cell deduced from the ED patterns is hardly visible on the HREM image, it is difficult to determine the exact structural arrangement of the ordering. The brighter spots in the rows corresponding to the La_2O_2 layers form an ordered array and, according to that, the placement of the fluorine atoms in the interstitial positions between two successive LaO could occur as shown in Fig. 5. The fluorine insertion leads to a tilting of the CuO_6 octahedra to increase the distance between the fluorine and the apical oxygen atoms. The cooperative character of this tilting may result in the appearance of the superstructure, visible on the ED patterns and the HREM image.

Samples synthesized at 300 and 400°C show similar structural aspects and will be discussed together. Two sections of reciprocal space are shown in Figs. 6a and 6b. The ED

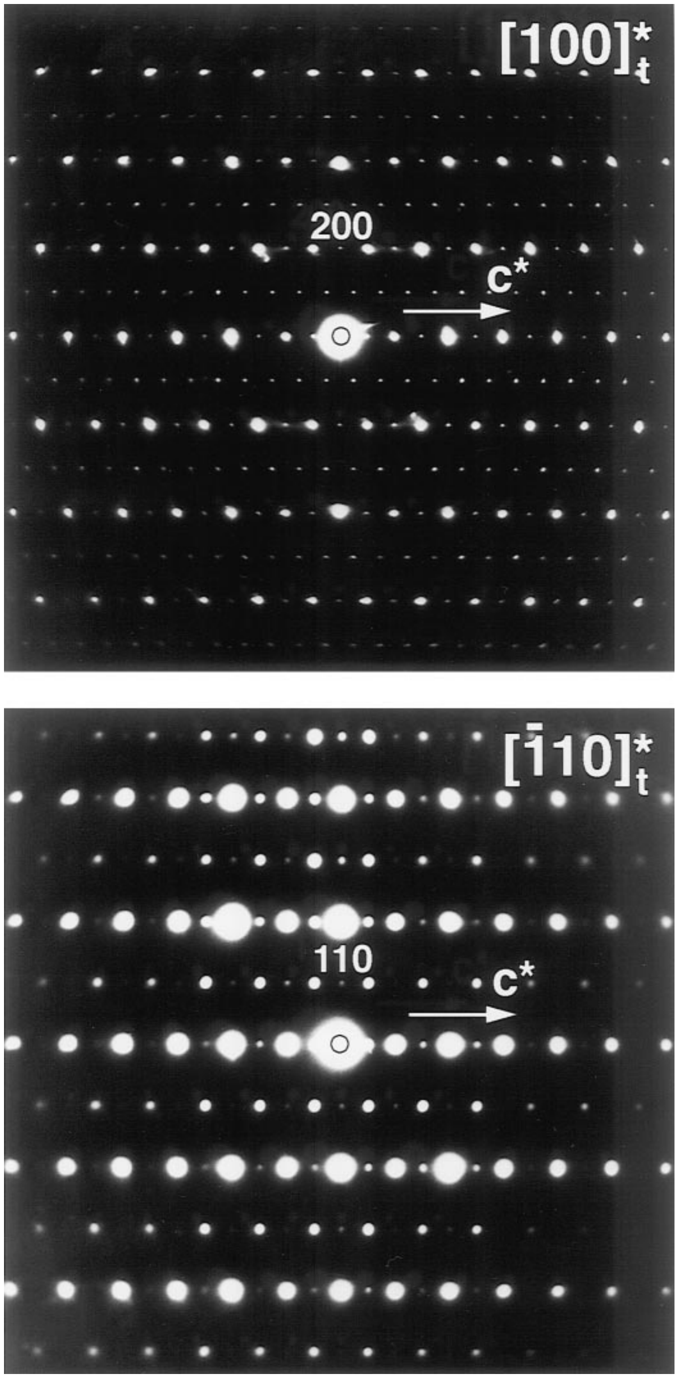

FIG. 3. Electron diffraction patterns taken along the most relevant zone axes of the sample prepared at 250°C fluorination.

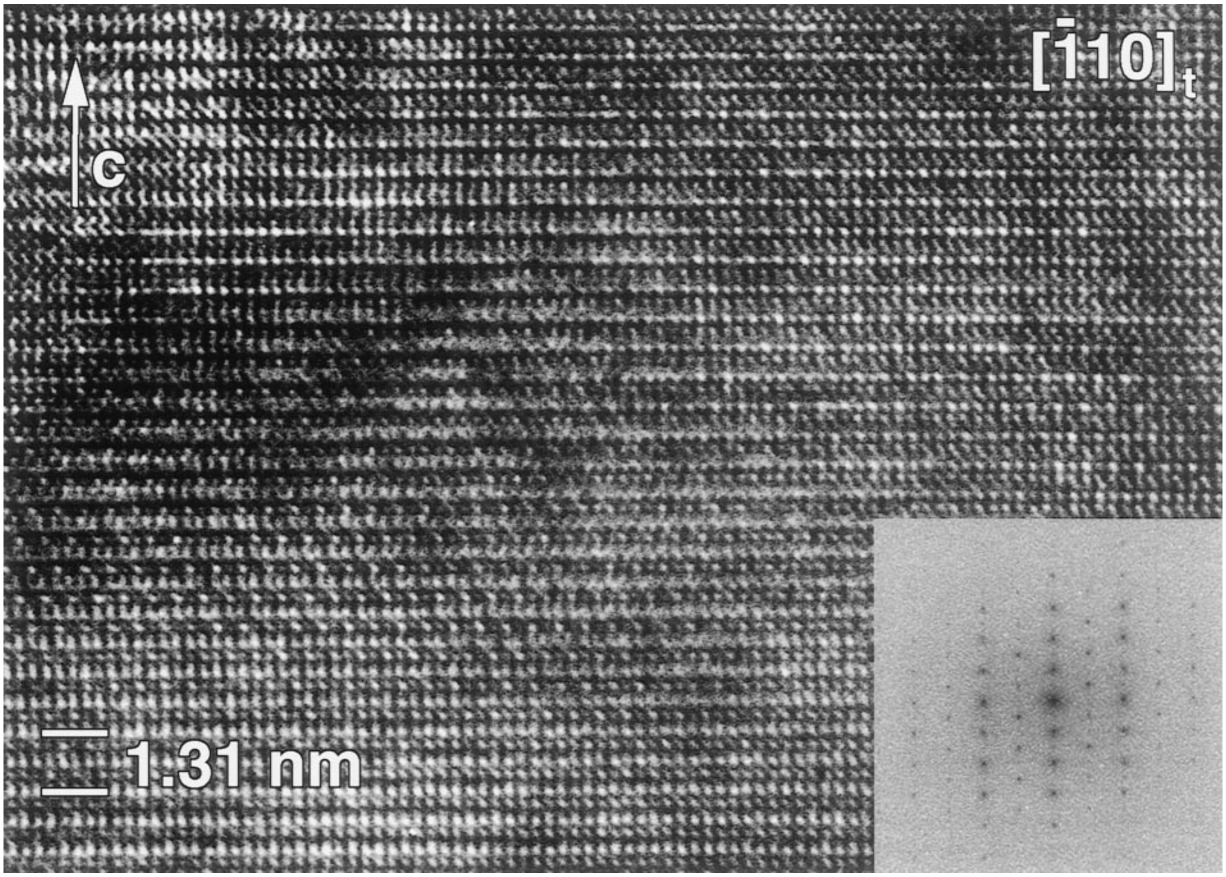

FIG. 4. $[\bar{1}10]_t$ HREM image for the sample fluorinated at 250°C. The optical diffraction pattern is shown as an inset.

pattern in Fig. 6a was taken along the $[\bar{1}10]_t^*$ zone axis of the K_2NiF_4 sublattice. The shortest reciprocal vectors, related to the superstructure reflections, are oriented along the $[116]_t^*$ and $[\bar{1}\bar{1}4]_t^*$ directions and form an approximately rectangular mesh with direct lattice dimensions 8.65×10.59 Å. However, the angle between the main vectors is not exactly 90°, which indicates a monoclinic symmetry for the superstructure. The $1/5[116]_t^*$ and $1/5[\bar{1}\bar{1}4]_t^*$ reciprocal vectors were chosen as respectively the $[100]_m^*$ and $[001]_m^*$ vectors of the monoclinic lattice, which makes it possible to index this diffraction pattern as the $[010]_m^*$ zone axis (the subscript index t refers to the K_2NiF_4-sublattice; m refers to the new monoclinic cell). The relative orientation of the subcell and supercell axes in reciprocal and direct space is shown in the insertion of Figs. 6a and 7, respectively. Since the $[\bar{1}10]_t^*$ and $[010]_m^*$ coincide, it is reasonable to assume that the repeat period along the *b* direction of the monoclinic cell is equal to the repeat period of the K_2NiF_4 sublattice along $[\bar{1}10]_t$ ($\approx$5.4–5.7 Å). Indeed, the ED pattern shown in Fig. 6b supports this assumption. Moreover, this pattern shows a doubling of the *a* parameter and the presence of systematic extinctions. Both ED patterns were completely indexed on the basis of a monoclinic unit cell with parameters $a \approx 17.36$ Å, $b \approx 5.62$ Å, $c \approx 10.59$ Å, and $\beta = 91.5$. The only extinction condition $h + k = 2n$ allows us to propose $C2$, Cm, and $C2/m$ as possible space groups. The relation between the K_2NiF_4-subcell and the

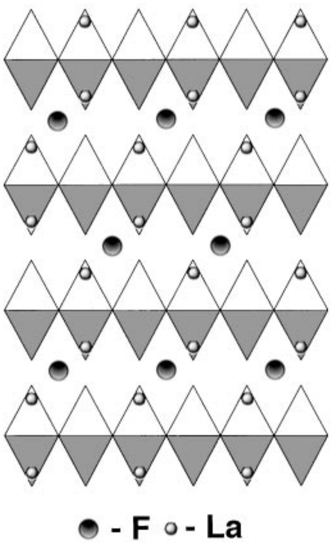

FIG. 5. Model of a possible fluorine distribution, in agreement with the HREM image in Fig. 4.

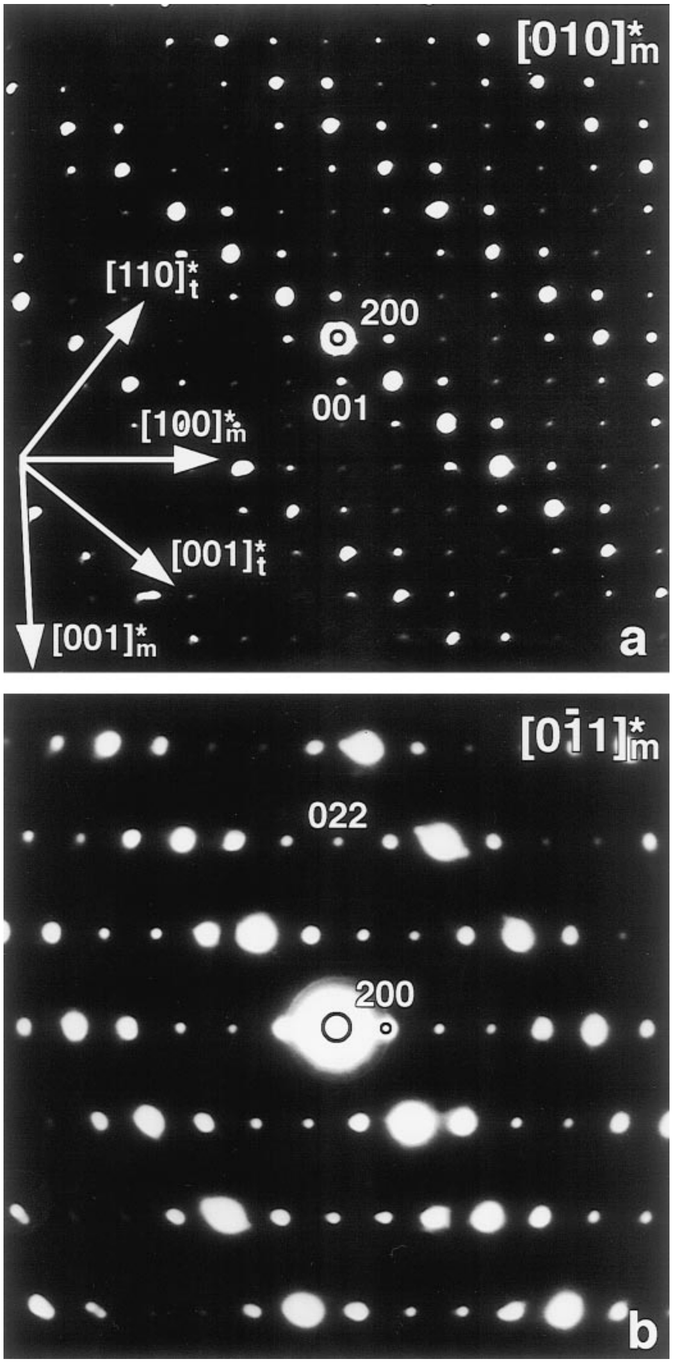

FIG. 6. Electron diffraction patterns of the monoclinic superstructure of the 300°C treated La_2CuO_4: $[010]^*_m$ (a) and $[0\bar{1}1]^*_m$ (b). The relative orientation of the reciprocal monoclinic axes and the vectors of K_2NiF_4 subcell is shown.

monoclinic supercell in reciprocal space is given by the following matrix:

$$h^*_m = 2h^*_t + 2k^*_t + l^*_t$$

$$k^*_m = -h^*_t + k^*_t$$

$$l^*_m = -3/2h^*_t - 3/2k^*_t + 1/2l^*_t.$$

The results of this reciprocal space investigation were confirmed by direct space observations. The HREM image, corresponding to the ED pattern of Fig. 6a, is shown in Fig. 8. According to image simulations (see below), the brighter rows can be interpreted as projections of the (CuO_2) planes, and the less bright rows in between as La_2O_2 layers. The superstructure is clearly visible due to an intensity variation along the La_2O_2 layers. Dark and bright areas alternate along $[110]_t$ and form an ordered array corresponding to the monoclinic unit cell described above. In the thicker part of the crystal (Fig. 8, bottom) it is clear that also the (CuO_2) planes are periodically affected by the formation of this superstructure.

Both the X-ray and the electron microscopy investigation reveal that the structure of all fluorinated compounds is based on a K_2NiF_4 subcell. This allows us to propose that the cation sublattice remains unchanged by fluorination and that the ordering appears to be due to insertion of additional anions and rearrangement between oxygen and fluorine atoms. Although it is difficult to determine the nature of the anion ordering unambiguously without neutron diffraction experiments, it is nevertheless possible to propose a probable model which is consistent with all ED and HREM results.

Since the main contrast variations were found to be linked to the La_2O_2 layers, the assumption that the (CuO_2) planes are not strongly affected by fluorine insertion seems quite reasonable. As it was found earlier, extra anions in R_2CuO_4 compounds with the T-type structure ($R = La$) are accommodated at interstitial cavities located between the two rocksalt LaO planes of the La_2O_2 layer (8, 9). These

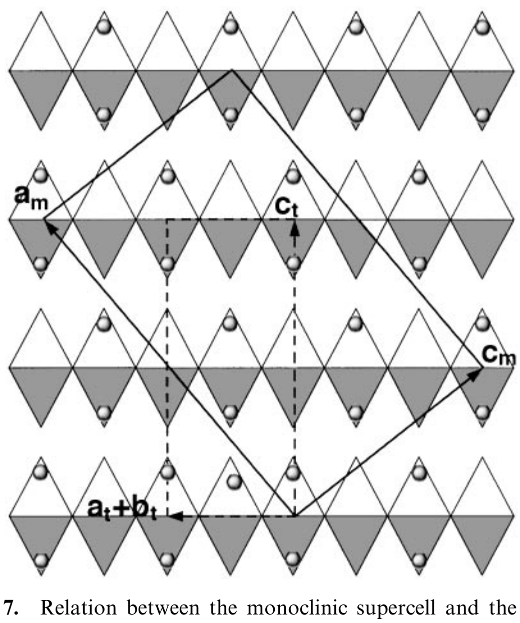

FIG. 7. Relation between the monoclinic supercell and the K_2NiF_4 subcell in direct space. The structure is represented along $[\bar{1}10]_t$.

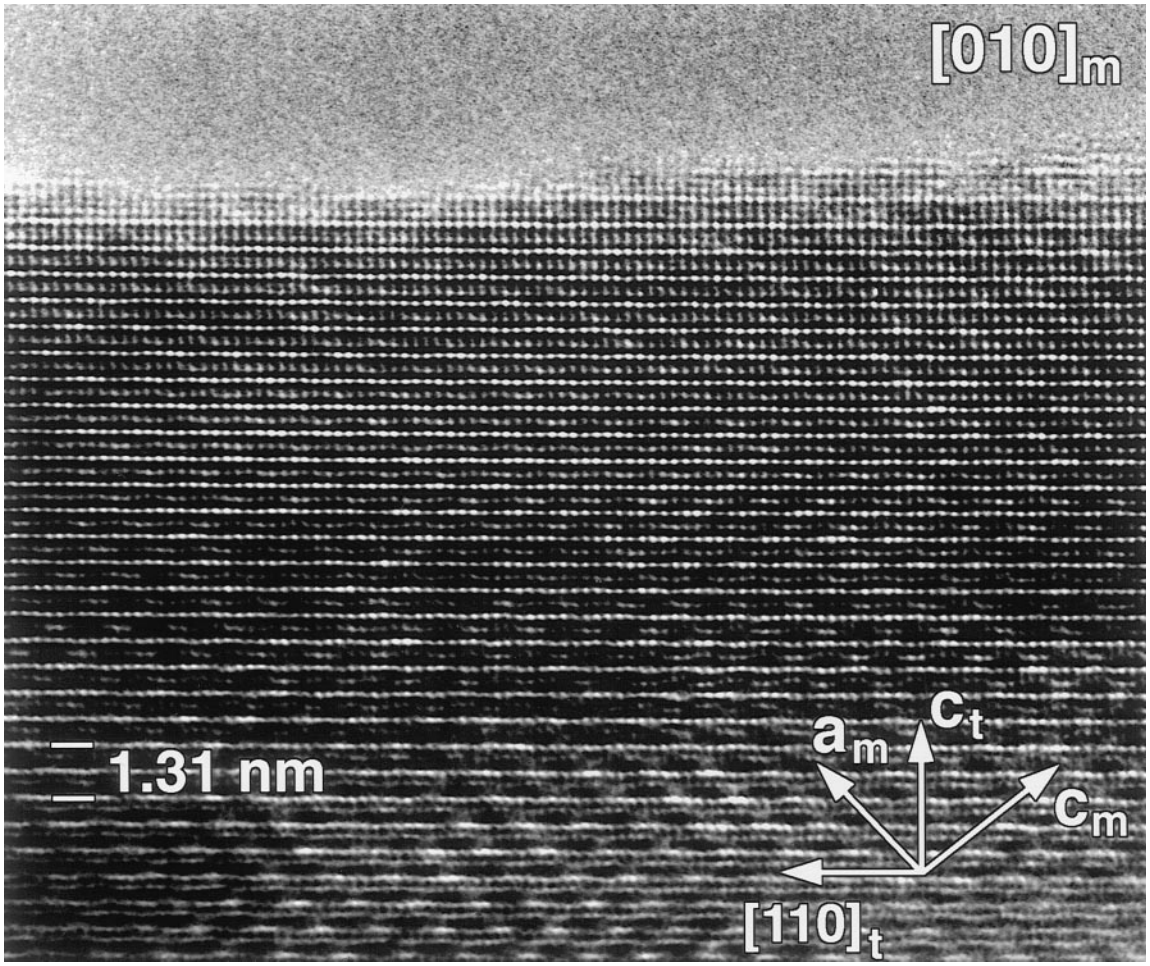

FIG. 8. HREM image along $[\bar{1}10]_t$ of the monoclinic superstructure, corresponding to the ED pattern shown in Fig. 6a.

cavities are coordinated by four La^{3+} ions and four apical oxygen atoms. The short distance between apical oxygen atoms and interstitial anions requires the displacement of apical oxygen or the removal of some of them. The fluorite-like structure of the R_2O_2 layers with fully occupied anion positions, tetrahedrally coordinated by R^{3+}, and without apical oxygen is realized for R_2CuO_4 compounds with T′-structure (R = Pr–Gd) (16). Thus the interstitial positions in the T-phase are the normal anion positions in the T′-phase. We propose that the blocks with fully occupied interstitial positions and without apical oxygen (fluorite slab) alternate with the blocks containing apical oxygen atoms and empty interstitial positions (rocksalt slab), resulting in a structure compatible with the experimentally observed image contrast. This means that part of the apical oxygen atoms in the initial La_2CuO_4 is replaced by interstitial fluorine. This competing anion exchange reaction always takes place during fluorination in a closed vessel at temperatures above 300°C, as was shown previously for different superconducting oxides (13, 14). The oxygen released due to anion exchange is absorbed at the inner surface of the copper tube, forming traces of Cu_2O. The cell parameters of the K_2NiF_4-subcell, determined by X-ray diffraction, also give an indirect confirmation of the anion exchange. The planar Cu–O distances, corresponding to $a = 4.038$ Å, are extremely large for Cu cations in the oxidation state between +2 and +3 and show a possible partial reduction of the (CuO_2) planes. The increased parameter $a = 4.038$ Å and decreased parameter $c = 13.093$ Å provide indirect support of the presence of fluorite slabs in the structure. Indeed, the phases with fluorite fragments (T′ and T*) have the significantly larger a parameter (and consequently a larger Cu–O in-plane bond length) than seen with La_2CuO_4. The transformation of the T-type structure into the T′ one is also accompanied by a significant compression of the unit cell along the c-axis. This is the case for the $La_{2-x}Nd_xCuO_{4+d}$ solid solution with T and T′ structures, where the values of the cell parameters for two close points could be compared. The T-phase ($x = 0.5$) exhibits cell parameters for the K_2NiF_4 subcell $a = 3.81$ Å and $c = 13.056$ Å; the T′ phase

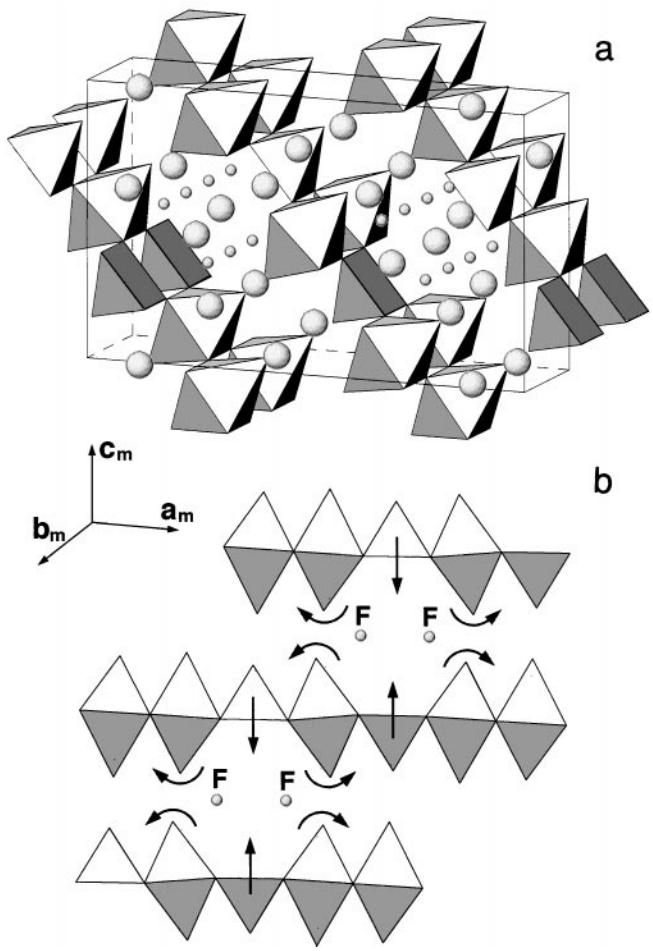

FIG. 9. Model for the anion ordering. (a) A 3D overview of the monoclinic supercell; Cu atoms are inside the octahedra and pyramids; large circles represent La atoms, small circles represent fluorine. (b) Projection of the unit cell along $[010]_m$; the cooperative atomic displacements are indicated by arrows; La atoms are not shown for clarity.

($x = 0.6$) has an increased parameter $a = 3.985$ Å and a decreased $c = 12.445$ Å (17).

The fitting between experimental HREM images and calculated ones computed using the structure models with different extensions of rocksalt and fluorite slabs long $(110)_t$ was tested. The best agreement with the experimental HREM image (shown in Fig. 8) was achieved with the model shown in Figs. 9a and 9b. The copper atoms above and below the fluorite slab are surrounded by five oxygen atoms forming a CuO_5 tetragonal pyramid. The CuO_6 octahedra on both sides of the inserted fluorine atoms are slightly tilted to increase the distance between the fluorine and the apical oxygen atoms in the neighboring rocksalt slabs. Due to this tilt, the CuO_5 pyramids are drawn closer to the fluorine, causing a modulation of the (CuO_2) planes which can be observed in the thicker part of experimental image. The atomic coordinates were calculated according to the determined monoclinic cell with the most symmetrical $C2/m$ space group. The calculated HREM images based on this model for different values of defocus and thickness are presented in Fig. 10.

The composition of this phase deduced from the structure model corresponds to the $La_2CuO_{3.6}F_{0.8}$ formula. This phase can be considered as a result of an anion exchange with replacing 0.4 O^{2-} anions by 0.8 F^- ones, which leads to a formal copper oxidation state $+2$. The disappearance of superconductivity for the samples obtained at 300–400°C fluorination can be understood by the insufficient formal copper valence as well as by the distortion of the (CuO_2) planes or by a partial anion replacement in the CuO_2 layers.

The structure of $La_2CuO_{3.6}F_{0.8}$ can be considered as intermediate between the T and T′ structures. The $c/3a$ ration for this phase is approximately equal to 1.08. This value is common for the T* phase which is a hybrid of the T and T′ phases with an alternation of rocksalt and fluorite blocks along the c-axis (18). However, in the $La_2CuO_{3.6}F_{0.8}$ compound the rocksalt and fluorite fragments also alternate along $[110]_t$, this in contrast to the T* structure. Unlike the fluorinated La_2CuO_4, the Cu–O in-plane distance in structures of different T* phases are average between T and T′. It was concluded from the analysis of a number of layered compounds that the Cu–O in-plane distance and a-parameter are usually determined by the size of the fluorite fragment (18). The in-plane Cu–O distances corresponding to $a = 4.038$ Å for $La_2CuO_{3.6}F_{0.8}$ are too large for the conventional T* phases and even bigger than in T′-phases, probably due to the occupation of the A-position in the fluorite slab by La atoms only and the larger ionic radius of La^{3+}.

It should be noted that the cell dimensions for the monoclinic superstructure differ significantly from those previously observed for the sample fluorinated at 230°C by F_2 (11). This is probably related to the different fluorinating agents used in both cases and to different temperatures of the treatment, which may lead to a different kind of anion ordering.

The relatively simple diffraction patterns, as shown in Figs. 6a and 6b were only occasionally met. Most of the crystallites produce more complicated ED patterns, which, however, could be interpreted as the superposition of different variants of the proposed monoclinic cell. Figure 11 reproduces the HREM image from part of a crystallite, containing a twinned monoclinic superstructure. Areas with opposite orientation of the monoclinic b axis are separated by a twin boundary lying in the $(001)_t$ plane. These areas alternate along $[001]_t$, producing a clearly different image contrast. In the right part of Fig. 11 a region without any superstructure (noted b) is observed; this corresponds to either the nonfluorinated initial La_2CuO_4 or a disordered placement of the fluorine and oxygen atoms. The inserted diffraction pattern can be unraveled as being due to superposition of the ED patterns along the $[010]^*_m$, $[0\bar{1}0]^*_m$, and $[\bar{1}10]^*_t$ zone axes.

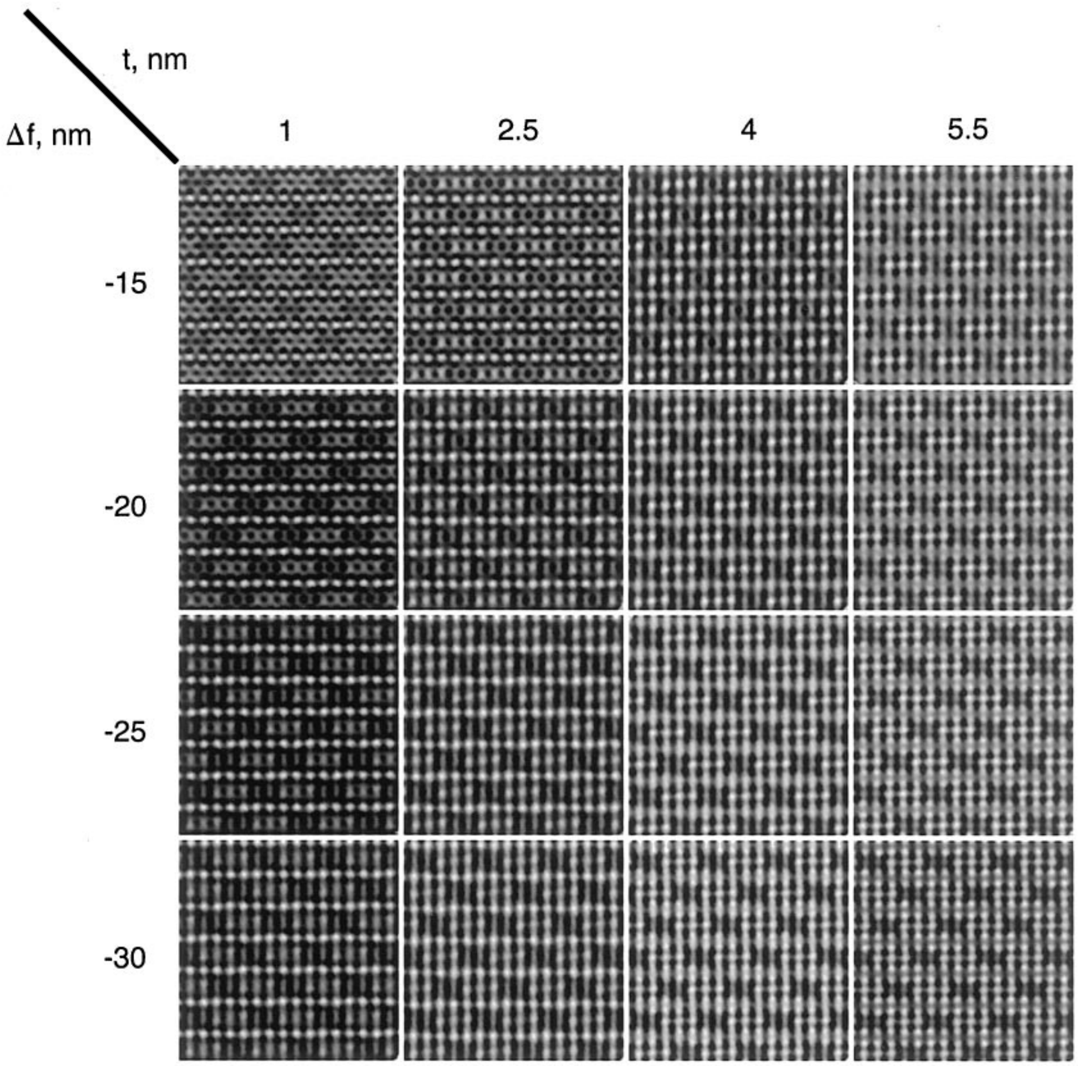

FIG. 10. Matrix of calculated HREM images along $[010]_m$ of the monoclinic superstructure.

Apart from the commensurate monoclinic superstructure, ED patterns exhibiting an incommensurate modulation of the La_2CuO_4 structure were also observed. The incommensurate modulation seen in Fig. 12 in the $[\bar{1}10]_t^*$ section can be described by a q-vector oriented approximately along the $[11\bar{3}]_t^*$ direction: $q = 0.12(a_t^* + b_t^*) - 0.38c_t^*$, and corresponds in real space to a wavelength $\lambda \approx 19$ Å. The HREM image shows dark stripes, separated by 19 Å. Similar incommensurate ED patterns and HREM images were observed before for La_2CuO_4 fluorinated at 200°C by F_2 [11], where this specific image contrast was connected to the presence of shear planes, parallel to $(112)_t$. According to the obvious similarity, the same model could also be applied for the interpretation of our HREM picture. A schematic model of the shear planes is shown in Fig. 13. The q-vector, determined from the ED pattern, defines the defect planes as being parallel to $(113)_t$. The wavelength of the modulation, 19 Å, indicates that these shear planes have to be repeated approximately every eight CuO_6 octahedra. The two parts of the structure on both sides of the shear plane are shifted with respect to each other by a displacement vector $R = [0, v, w]$. However, due to the lack of resolution, the exact value of this displacement as well as the detailed structure of these shear planes are not as clear as in the case of shear structures in oxygen deficient La_2CuO_{4-x} (19). The reason for the inferior quality of the image is due to the limited stability of the incommensurate structure under the electron beam.

CONCLUSIONS

The present investigation evidences the following sequence changes related to an increasing fluorine content in fluorinated La_2CuO_4.

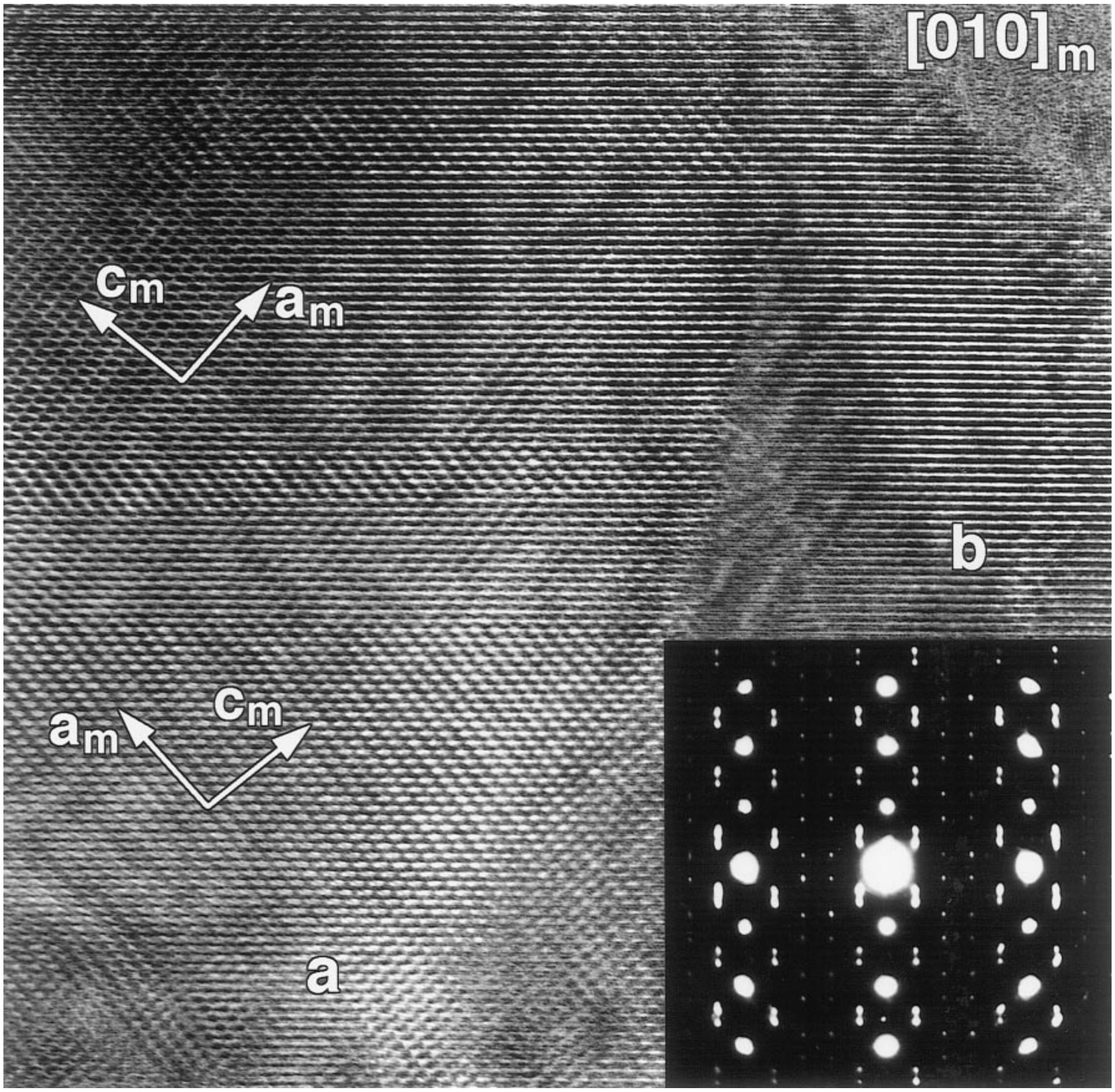

FIG. 11. HREM image showing a twinned region of the monoclinic superstructure (a) and a region without anion ordering (b). The corresponding ED pattern is shown as an inset.

(i) A first stage of fluorine insertion takes place at a low fluorination level and at a low temperature of about 200°C. At this stage a small amount of fluorine (up to $La_2Cu(O,F)_{4.18}$) (7)) enters into the interstitial positions between the double LaO layers causing an increase of the orthorhombic distortion of the unit cell. This leads to an increased formal copper valence and the appearance of superconductivity with T_c up to 40 K. No ordering of interstitial anions is found in this compound.

(ii) Fluorination at 250°C leads to a structural transformation with the formation of a K_2NiF_4-type unit cell. Electron microscopy reveals a superstructure consisting of a body-centered tetragonal lattice with doubled cell parameters of the K_2NiF_4-subcell which arises from an alternation of vacant and filled interstitial positions along $[001]_t$ and $[110]_t$. A cooperative tilting of the CuO_6 octahedra could be proposed as a possible reason for the anion ordering.

(iii) The anion exchange becomes the predominant reaction when the fluorination temperature increases above 300°C. The fluorine atoms occupy interstitial positions with the removal of neighboring apical oxygen resulting in the transformation of part of the CuO_6 octahedra into CuO_5 pyramids. Blocks with occupied interstitial positions and removed apical oxygens (fluorite slabs) alternate with the blocks of rocksalt slabs in an ordered manner, leading to a new monoclinic phase with ideal composition $La_2CuO_{3.6}F_{0.8}$.

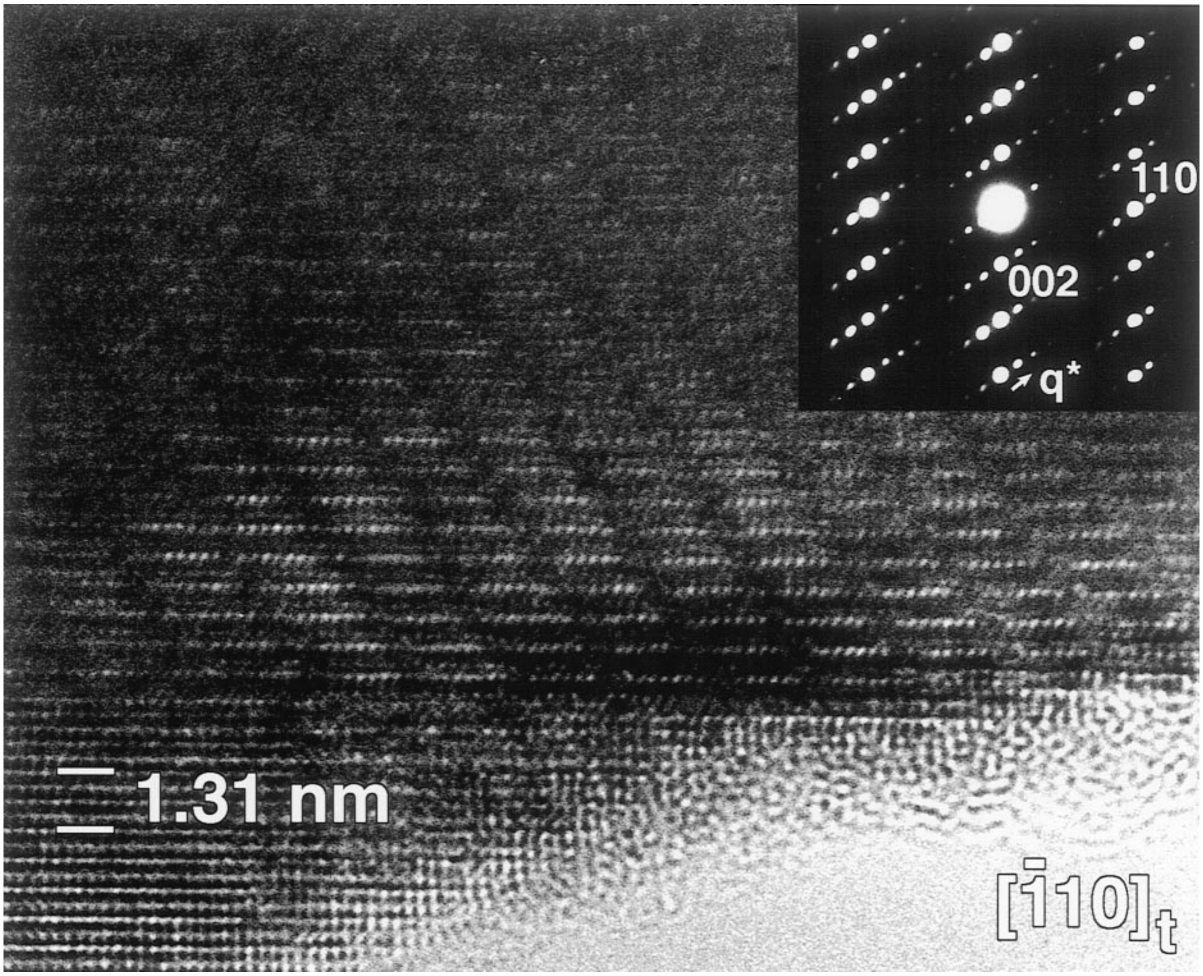

FIG. 12. HREM image and ED pattern of the incommensurate superstructure along $[\bar{1}10]_t$.

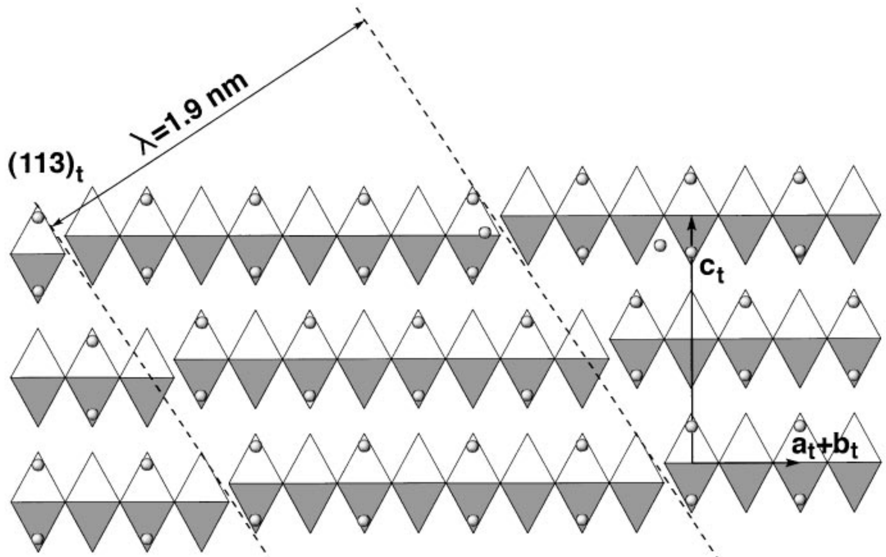

FIG. 13. Schematic model of the modulated structure shown in Fig. 12. The main vectors of the K_2NiF_4 subcell in the foil plain are indicated. R is the displacement vector and λ is the wavelength of the modulation.

ACKNOWLEDGMENTS

Dr. O. I. Lebedev, Dr. M. G. Rozova, and Dr. E. M. Kopnin are acknowledged for help with EM, sample preparation, and structural discussions, respectively. The authors are also grateful to P. E. Kazin for magnetic measurements and to V. B. Sokolov for XeF_2. This work has been performed in the framework of a NATO Grant HTECH.LG 960325 and IUAP-PAI 4/10 of the Belgian government. The work is partially supported by the Russian Scientific Council on Superconductivity (Poisk), INTAS-932483ext, and RFBR-INTAS (00639 I-96). A. Abakumov is grateful to DWTC (Belgium) for financial support.

REFERENCES

1. J. B. Bednorz and K. A. Muller, *Z. Phys. B* **64,** 189 (1986).
2. J. E. Shriber, B. Morosin, R. M. Merill, P. F. Hlava, E. L. Venturini, J. F. Kwak, P. J. Nigrey, R. J. Baughman, and D. S. Ginley, *Physica C* **152,** 121 (1988).
3. G. Demazeau, F. Tresse, Th. Plante, B. Chevalier, J. Etorneau, C. Michel, M. Hervieu, B. Raveau, P. Lejay, A. Sulpice, and R. Tournier, *Physica C* **153,** 824 (1988).
4. E. Takayama-Muromachi, T. Sasaki, and Y. Matsui, *Physica C* **207,** 97 (1993).
5. E. Takayama-Muromachi and A. Navrotsky, *Physica C* **218,** 164 (1993).
6. B. M. Tissue, K. M. Cirillo, J. C. Wright, M. Daeumling, and D. C. Larbalestier, *Solid State Commun.* **65,** 51 (1988).
7. B. Chevalier, A. Tressaud, B. Lepine, K. Amine, J. M. Dance, L. Lozano, E. Hickey, and J. Etourneau, *Physica C* **167,** 97 (1990).
8. M. H. Tuilier, B. Chevalier, A. Tressaud, C. Brisson, J. L. Soubeyroux, and J. Etourneau, *Physica C* **200,** 113 (1992).
9. C. Chaillout, S. W. Cheong, Z. Fisk, M. S. Lehmann, M. Marezio, B. Morozin, and J. E. Schriber, *Physica C* **158,** 183 (1989).
10. B. Chevalier, A. Tressaud, B. Lepine, C. Robin, and J. Etourneau, *J. Less Common Metals* **164,** 832 (1990).
11. F. Weill, B. Chevalier, M. Chambon, A. Tressaud, B. Darriet, J. Etourneau, and G. Van Tendeloo, *Eur. J. Solid State Inorg. Chem.* **30,** 1095 (1993).
12. E. I. Ardashnikova, S. V. Lubarsky, D. I. Denisenko, R. V. Shpanchenko, E. V. Antipov, and G. Van Tendeloo, *Physica C* **253,** 259 (1995).
13. R. V. Shpanchenko, M. G. Rozova, A. M. Abakumov, E. I. Ardashnikova, M. L. Kovba, S. N. Putilin, E. V. Antipov, O. I. Lebedev, and G. Van Tendeloo, *Physica C* **280,** 272 (1997).
14. A. M. Abakumov, M. G. Rozova, R. V. Shpanchenko, M. L. Kovba, S. N. Putilin, E. V. Antipov, O. I. Lebedev, G. Van Tendeloo, E. M. Kopnin, and J. Karpinski, *Physica C*, in press.
15. A. M. Abakumov, V. L. Aksenov, V. A. Alyoshin, E. V. Antipov, A. M. Balagurov, D. A. Mikhailova, S. N. Putilin, and M. G. Rozova, *Phys. Rev. Lett.* **80,** 385 (1998).
16. P. Lightfoot, S. Pei, J. D. Jorgensen, X.-X. Tang, A. Manthiram, and J. B. Coodenough, *Physica C* **169,** 15 (1990).
17. F. Arrouy, A. Wattiaux, C. Cros, G. Demazeau, J.-C. Grenier, M. Pouchard, and J. Etourneau, *Physica C* **175,** 342 (1991).
18. A. Abakumov, E. Antipov, L. Kovba, E. Kopnin, S. Putilin, and R. Shpanchenko, *Russ. Chem. Rev.* **64,** 719 (1995).
19. G. Van Tendeloo and S. Amelinckx, *Physica C* **176,** 575 (1991).